THE ASTROPHYSICAL JOURNAL, 426:123–130, 1994 May 1

A VERY METAL POOR H II REGION IN THE OUTER DISK OF M101[1,2]

DONALD R. GARNETT[3]
Astronomy Department, Univeristy of Minnesota, 116 Church Street, SE, Minneapolis, MN 55455
AND
ROBERT C. KENNICUTT, JR.[4]
Steward Observatory, University of Arizona, Tucson, AZ 85721
Received 1993 June 24; accepted 1993 November 4

ABSTRACT

We present new spectroscopic observations of an H II region in the extreme outer disk of the spiral galaxy M101, more than 32 kpc from the nucleus, or 25% farther out than the well-studied giant H II region NGC 5471. From a derived [O III] electron temperature of 13,900 K, we derive log O/H = −4.1, only 10% of the solar value, and smaller than the abundance measured in NGC 5471. Log N/O = −1.49, similar to the values seen in metal-poor dwarf galaxies, while log S/O = −1.74, essentially identical to the solar value, confirming the trend of constant S/O observed in earlier studies. With the inclusion of this new object, the composition gradient in M101 from published spectroscopic observations shows no evidence for either a break in the gradient from 4 to 33 kpc, or a rise in the abundances in the outer parts of the disk.

Subject headings: galaxies: individual (M101) — galaxies: spiral — H II regions — ISM: abundances

1. INTRODUCTION

Blair, Kirshner, & Chevalier (1982) emphasized the importance of extensive radial coverage in comparing composition gradients across spiral disks. Despite this caution, the outer disks of spirals (especially beyond the 25 mag arcsec^{-1} photometric radius R_{25}) remain relatively unexplored. This may be due in part to a lack of narrow-band imaging of such regions in nearby galaxies, which have large angular sizes compared to typical CCD imager fields, and to a dearth of luminous H II regions suitable for spectroscopic study at large galactocentric distances. Whatever the reason, a search for and study of extreme outer disk H II regions would be profitable, not only for defining abundance gradients, but also for comparing the evolution of spiral disks and irregular galaxies in comparable environments (low metallicity and low surface brightness) and in studying star formation in such low-density environments. Garnett & Shields (1987) observed an H II region at R/R_{25} = 1.3 in M81, which played a key role in defining the composition gradient in that galaxy. More recently, Garnett, Odewahn, & Skillman (1992) studied the nebula MA 1 in M33 at R/R_{25} = 1.1, which had been identified as a possible optically thin nebula by McCall, Rybiski, & Shields (1985), but which in reality turned out to be one of the most metal-poor H II regions ever observed in a spiral galaxy.

Sedwick & Aller (1981) identified another relatively bright H II region (their region "O") roughly 15′ north of the nucleus of M101. The nebula is also number 681 in the list of H II regions from Hodge et al. (1990), and hereafter we will refer to the nebula as H681. An identification chart for H681 can be found in Figure 14 of Hodge et al. (1990). Hodge et al. list the approximate position of H681 as $14^h03^m13^s.7$, +54°35′47″ (2000.0), which corresponds to offsets of approximately 7″ east and 884″ north of the galactic nucleus. The region is located near the north end of an outer stellar and H I spiral arm in M101. H I 21 cm line emission was detected at the position of H681, but no 21 cm continuum (Viallefond, Allen, & Goss 1981; they identify the H I source as Goss I). At a radial distance of 32.6 kpc from the nucleus of M101 (assuming the distance to M101 is 7.4 Mpc, from Sandage & Tammann 1976), H681 is about 25% farther out than the well-known giant H II region NGC 5471. This corresponds to R/R_{25} = 1.05, where R_{25} = 28′.8 from RC3 (de Vaucouleurs et al. 1991). Garnett & H. Dinerstein (unpublished) obtained an IDS spectrum of H681 at McDonald Observatory in 1986; the spectrum showed [O II] and [O III] line strengths consistent with log O/H ≈ −4.4, much smaller than had been observed previously in a spiral galaxy. Unfortunately, spectrograph focusing problems prevented them from detecting the [O III] 4363 Å line, and so they were unable to measure the electron temperature directly to confirm the abundance estimate. As part of a larger survey of H II regions in M101, we obtained a blue CCD spectrum in 1989 with the Steward Observatory 2.3 m reflector. That spectrum showed the 4363 Å line, giving a preliminary temperature and abundance which supported the earlier conjecture of Garnett & Dinerstein. Motivated by these results, we recently obtained new, high resolution blue CCD spectra and a complementary red spectrum of this object with the MMT, and we present the results here.

2. OBSERVATIONS AND ANALYSIS

2.1. *Observations*

We have used narrow-band CCD observations of M101 to measure the Hα flux of H681, The images were obtained in 1989 May by R. Kennicutt, R. Walterbos, and R. Braun using the Burrell Schmidt telescope at KPNO, equipped with a Tektronix 512 × 512 CCD detector. Images were obtained through filters centered on Hα and the neighboring continuum,

[1] Observations reported here were obtained in part at the Multiple Mirror Telescope Observatory, a joint facility of the University of Arizona and the Smithsonian Institution.
[2] Observations made with the Burrell Schmidt of the Warner and Swasey Observatory, Case Western Reserve University.
[3] Hubble Fellow.
[4] Visiting Astronomer, Kitt Peak National Observatory, National Optical Astronomy Observatories, operated by the Association of Universities for Research in Astronomy, Inc., under cooperative agreement with the National Science Foundation.

and calibrated using aperture photometry of NGC 5461, NGC 5462, and NGC 5471 from Kennicutt (1978). These yield Hα fluxes of $1.1 \pm 0.1 \times 10^{-13}$ ergs cm^{-2} s^{-1} for the central 15″ core, and $1.6 \pm 0.15 \times 10^{-13}$ ergs cm^{-2} s^{-1} for the entire complex. These values correspond to Hα luminosities of 0.7–1.0×10^{39} ergs s^{-1}, and ionizing luminosities of 5–7×10^{50} photons s^{-1}, for an assumed distance of 7.4 Mpc. This is comparable to large Galactic H II regions such as the Carina nebula (Kennicutt 1984), and implies that H681 is probably ionized by a large OB association. However, this is still 25–40 times fainter than the brightest H II complexes in M101 (e.g., NGC 5461, NGC 5471), which, along with its much lower surface brightness, probably accounts for why it has not been well studied previously. H681 is poorly resolved in our images, but the data indicate a low surface brightness core surrounded by other emission peaks. Such diffuse (and sometimes ringlike) structures are common among H II regions in the extreme outer disks of nearby galaxies such as M31, M33, and the LMC.

Spectra of H681 were obtained using the Red Channel spectrograph on the 4.5 m Multiple Mirror Telescope (MMT). Three grating setups were used to cover the spectral range 3600–10,000 Å. Two sets of spectra were obtained in the blue, using a 2″ × 180″ slit and a thinned Loral 800 × 1200 CCD detector. These provided coverage of 3600–5200 Å at 8 Å resolution (to measure the strong [O II], [O III], and Balmer lines), and 4200–5100 Å at 4 Å resolution (to obtain high signal/noise measurements of the weak [O III] 4363 Å and He I 4471 Å lines). In addition, we used the Red Channel spectrograph with a cross-dispersed echellette grating to observe the 4600–10,000 Å in five overlapping orders, at spectral resolutions of 7–10 Å. In this case a 2″ × 20″ slit was used with a TI 800 × 800 element CCD detector.

For all observations the position of the spectrograph slit was oriented east–west, and centered on the brightest continuum region visible on the acquisition TV. There is good agreement between the emission distributions along the slit in our measurements which, combined with the agreement in relative line ratios (below), confirms that the pointing was consistent in the different setups. Following the data reductions, we extracted and collapsed 6″ long sections of the slit, centered on the brightest emission-line region, for analysis. This choice was motivated by the echellette data, for which the slit length was not long enough to cover the entire nebula. For comparison, we also extracted 6″ and 18″ segments of the blue spectra centered on the continuum. Figure 1 shows our high-dispersion blue spectrum.

We analyzed the three MMT spectra independently rather than combining them into a single spectrum. We measured emission-line fluxes using both direct integration and Gaussian line fits. The [O III] 4363 Å line was well separated from Hγ in our high-dispersion blue spectrum and easily measured, as can be seen in Figure 1; however, we also used the Hγ line profile as a template for fitting the 4363 Å line. The differences between the measurements using direct integration and those from Gaussian fits were small enough to be negligible. The red spectrum was scaled to the blue via the [O III]/Hβ line ratios, which agree to within 1% between the blue and red. Our quoted uncertainties in relative line strengths were determined from the quadratic sum of the uncertainties arising from the signal-to-noise ratio in the lines, flat-field fluctuations, and the flux calibration. There were significant differences in absolute line fluxes and slight differences in the derived interstellar extinction coefficients among the three spectra, which may signify slight changes in pointing or clouds. However, the [O III]/Hβ ratios for all three spectra compare very well (within 1%), so we are confident that the relative line strengths across the spectra are accurate.

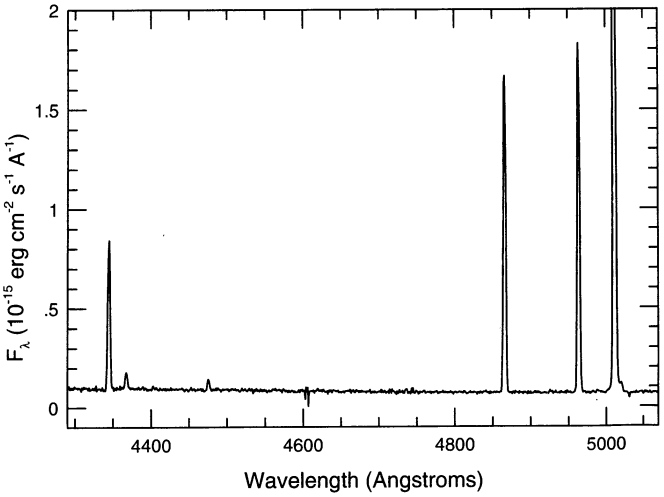

FIG. 1.—High-dispersion MMT spectrum of H681, showing clearly our detection of the [O III] 4363 Å and He I 4471 Å lines.

The logarithmic extinction at Hβ, C(Hβ) was determined independently for each spectrum by comparing the observed Balmer decrement with the theoretical Balmer decrement (Hummer & Storey 1987) for $T_e = 14{,}000$ K, the temperature estimated from the observed, uncorrected [O III] λ5007/λ4363 line ratio. We corrected for underlying stellar Balmer absorption using a constant absorption equivalent width of 2 Å, similar to that determined empirically by McCall et al. (1985). The remaining emission lines in each spectrum were corrected for interstellar extinction using the extinction coefficients listed in Table 1 and the average interstellar extinction curve from Osterbrock (1989). Our observed line strengths, both uncorrected and corrected for extinction and Balmer absorption, normalized to the Hβ flux, are listed in Table 1.

2.2. *Electron Densities and Temperatures*

We estimated the electron density n_e from the ratio of the [S II] 6717 Å and 6731 Å lines from a five-level atom calculation, using the estimated electron temperature of 14,000 K. We derive $n_e = 300$ $(+600;\ -300)$ cm^{-3}. The observed doublet ratio lies near the low-density limit for [S II] and the [S II] lines are weak in this object, so our estimate of n_e is relatively uncertain. Nevertheless, the estimated electron density is low enough that collisional effects introduce less than 10% uncertainty in the derived abundances.

The electron temperature T_e was computed from the dereddened intensity ratio of [O III] (λ4959 + λ5007) to [O III] λ4363, again using the five-level atom approximation. We obtain $T_e = 13{,}900$ $(+600;\ -400)$ K from the observed line ratio of 81.3 ± 7.1, the weighted mean of the low-dispersion and high-dispersion blue measurements. Our spectra provided six independent measurements of the T_e, and the quoted uncertainty indicates the excellent agreement between these measurements.

2.3. *Ionic and Elemental Abundances*

Ionic abundances relative to hydrogen were computed from the observed emission-line strengths and the derived T_e and n_e,

TABLE 1

LINE INTENSITIES FOR H681[a]

LINE	LOW DISPERSION BLUE		HIGH DISPERSION BLUE		ECHELLETTE	
	I_o	I_c	I_o	I_c	I_o	I_c
[O II] λ3727	2.171 (0.095)	2.442 (0.158)	...	...	...	...
[Ne III] λ3869	0.245 (0.040)	0.265 (0.065)	...	...	...	...
Hδ	0.233 (0.015)	0.252 (0.031)	...	...	...	...
Hγ	0.447 (0.021)	0.472 (0.040)	0.468 (0.021)	0.472 (0.032)	...	...
[O III] λ4363	0.049 (0.006)	0.052 (0.007)	0.050 (0.004)	0.050 (0.005)	...	...
He I λ4471	0.028 (0.005)	0.029 (0.005)	0.028 (0.003)	0.028 (0.003)	...	...
Hβ	1.000	1.000	1.000	1.000	1.000	1.000
[O III] λ4959	1.023 (0.045)	1.010 (0.047)	1.058 (0.045)	1.056 (0.047)	1.033 (0.067)	1.015 (0.066)
[O III] λ5007	3.099 (0.134)	3.054 (0.142)	3.130 (0.133)	3.122 (0.138)	3.114 (0.183)	3.052 (0.181)
He I λ5876	...	...	...	...	0.091 (0.015)	0.078 (0.013)
[O I] λ6300	...	...	...	...	<0.028	<0.024
Hα	...	...	...	...	3.475 (0.202)	2.808 (0.225)
[N II] λ6583	...	...	...	...	0.134 (0.029)	0.108 (0.024)
He I λ6678	...	...	...	...	0.029 (0.013)	0.023 (0.011)
[S II] λ6717	...	...	...	...	0.181 (0.023)	0.145 (0.020)
[S II] λ6731	...	...	...	...	0.155 (0.022)	0.124 (0.019)
[S III] λ9069	...	...	...	...	0.166 (0.019)	0.113 (0.016)
[S III] λ9532	...	...	...	...	0.430 (0.044)	0.251[b] (0.038)
$W(H\beta)$[c]	85.5		88.0		120	
$W(H\gamma)$[c]	27.2		29.7		...	
$W(H\delta)$[c]	9.1		...		...	
$W(\lambda 4471)$[c]	1.9		2.0		...	
$W(\lambda 5876)$[c]	...		...		19.2	
$W(\lambda 6678)$[c]	...		...		10.3	
$C(H\beta)$	0.18 (0.04)		0.03 (0.005)		0.25 (0.02)	

[a] Observed (I_o) and corrected (I_c) line strengths relative to Hβ, with 1 σ uncertainties given in parentheses.
[b] Corrected for contribution from Paschen 8 λ9546.
[c] Emission line equivalent width in angstroms.

using line emissivities calculated with the five-level atom program; for [O III], we used the weighted average of our three separate measurements. Since both observations and photoionization calculations suggest that H II regions are not isothermal, we use the prescriptions in Garnett (1992) to derive mean electron temperatures for different ions based on the observed [O III] temperature. Thus, for O^{+2} we use the [O III] temperature, while for O^+, N^+, and S^+, we use $T = 12{,}700$ K, and for S^{+2} we use $T = 13{,}200$ K. The spread in photoionization model results leads to an uncertainty of 500 K or less in these estimated temperatures, in addition to the uncertainty in the measured [O III] temperature. Our computed ionic abundances are listed in Table 2.

Determination of the elemental abundances requires summing of the ionic abundances for each element, taking into account any important unobserved ionization states. We observe both of the important ionization states for oxygen, so $O/H = O^+/H^+ + O^{+2}/H^+$. We assume $N/O = N^+/O^+$ to estimate the total nitrogen abundance (Peimbert & Costero 1969); Garnett (1990) suggested that this approximation is probably accurate to ±20% for O/H < 25% solar, although there is some observational evidence that this may not be true at higher abundances. For sulfur, the models of Garnett (1989) indicate a small ionization correction for S^{+3}, of order 10%. Our estimated abundances for O, N, and S are listed in Table 2.

Determining the helium abundance involves greater uncertainties. We have calculated He^+/H^+ from the He I λ4471, λ5876, and λ6678 line strengths in our three spectra. Before the He/H ratio can be estimated, there are a number of systematic uncertainties that need to be addressed. First, our best-measured line, λ4471, has a small equivalent width. Thus, underlying stellar absorption in the He I lines could have a significant effect on the line strengths. Olofsson (1993) has computed synthetic spectra for starbursts to estimate the effect of stellar He I absorption on helium abundance determinations in H II regions. He finds that the λ4471 equivalent width reaches a maximum of 0.35 Å for young starbursts with reasonable parameters. No comparable calculations are available for the 5876 Å and 6678 Å lines; however, an examination of observed

TABLE 2

IONIC AND ELEMENTAL ABUNDANCES

Species	Abundance
He^+/H^+	0.070 ± 0.007
ICF	1.05 ± 0.10
He/H	0.074 ± 0.010
O^+/H^+	$(3.8 \pm 1.0) \times 10^{-5}$
O^{+2}/H^+	$(4.6 \pm 0.5) \times 10^{-5}$
ICF	1.00
O/H	$(8.4 \pm 2.0) \times 10^{-5}$
N^+/H^+	$(1.2 \pm 0.3) \times 10^{-6}$
N^+/O^+	$(3.2 \pm 1.2) \times 10^{-2}$
Ne^{+2}/H^+	$(6.9 \pm 2.6) \times 10^{-6}$
Ne^{+2}/O^{+2}	0.15 ± 0.06
S^+/H^+	$(4.8 \pm 0.6) \times 10^{-7}$
S^{+2}/H^+	$(8.5 \pm 1.4) \times 10^{-7}$
ICF	1.1
S/H	$(1.5 \pm 0.3) \times 10^{-6}$
log N/O	-1.49 ± 0.14
log S/O	-1.74 ± 0.12

He I equivalent widths in O stars (Conti 1973, 1974; Conti & Frost 1977) suggests that one can reasonably assume a λ5876 equivalent width twice that for λ4471, while the λ6678 line is generally of similar strength or weaker than λ4471. Therefore, we correct our λ4471 and λ6678 line strengths for 0.3 Å of underlying absorption, and 0.6 Å underlying absorption for the λ5876 line. The corrections amounted to about 15% for λ4471, but less than 5% for λ5876 and λ6678. Collisional excitation also systematically increases the He I line strengths (see Clegg 1987, for example). At our observed electron temperature and density, the collisional contribution is of order 10% or less for each line, smaller than the observational uncertainties, and we choose to neglect it. It suffices to note that the collisional correction would reduce our derived helium abundance. The radial velocity of M101 is such that we should not expect significant absorption of λ5876 by Galactic interstellar Na D; in any case, the consistency of our derived He^+ abundances suggest that such absorption should be small, less than 10%. We list in Table 2 the average of the He^+/H^+ ratios, corrected for underlying stellar absorption, from each of our measurements of λ4471, λ5876, and λ6678, weighted by the uncertainties in the line strengths.

The relatively high O^+/O fraction in H681 indicates that we need to consider the presence of neutral He in the H^+ region. This is a matter of considerable controversy (Shields 1987), and a number of schemes have been devised to estimate this correction. We consider first the "radiation softness" parameter $\eta = (O^+/O^{++})/(S^+/S^{++})$ discussed by Vílchez & Pagel (1988); the ionization correction schemes of Mathis (1982) give similar results. Following Pagel et al. (1992), our measured $\eta = 1.48$ combined with the photoionization models of Stasińska (1990) indicates a negligible contribution from neutral helium, and lies within the range of giant H II regions ionized by hot O stars (Vílchez & Pagel 1988). However, it has been pointed out that the relatively high [O II]/[O III] and [S II]/[S III] ratios observed in H681 are not consistent with Stasińska's metal-poor H II region models. A supernova remnant (SNR) superposed on the H II region could produce the relatively strong [S II] emission (Skillman 1985); however, our low 3 σ upper limit of 0.024 for [O I]/Hβ and the lack of strong radio continuum emission from H681 (Viallefond et al. 1981) rule out the presence of a bright SNR. Therefore, we have computed some of our own photoionization models to explore the problem further.

We started with a set of uniform-density filled sphere models, computed using the nebula code of Shields (see Garnett 1989, 1990 for details). From our observed Hα flux and nebular diameter of about 540 pc (15″ at the distance of M101), we estimate an rms density of about 1 cm^{-3}. We used this density, our estimated $N(\mathrm{Lyc}) \approx 7 \times 10^{50}$ photons s^{-1} and the derived nebular abundances as input to the models. The input ionizing continuum fluxes were taken from the non-LTE models of Mihalas (1972) for effective temperatures of 35,000, 37,000, 40,000, and 50,000 K. These filled sphere models suggested that the observed line strengths of [O II], [O III], [Ne III], and [S III] could be matched with a stellar effective temperature of 36,000–37,000 K. However, none of the filled-sphere models could reproduce the high [S II] strengths, and there was little variation of the [S II] strengths between the models.

As noted earlier, H681 is large and diffuse. From the Hα imaging we derive a peak emission measure of only 800–1000 pc cm^{-6}, much smaller than typical values for giant H II regions (Kennicutt 1984). This led us to consider models in which the assumption of a uniformly filled sphere is relaxed. We computed another set of models in which we treated the nebula as a thin spherical shell (essentially plane-parallel geometry) with a uniform density. The input for the shell models were the same as the spherical models above, except that the starting radius of the models was fixed at 8×10^{20} cm and we used higher gas densities (3 and 10 cm^{-3}), to give an outer radius close to the observed nebular size. The shell models gave systematically higher [S II]/Hβ and [S II]/[S III] line ratios and a lower degree of ionization than the corresponding spherical models. Although none of the models we computed gave a precise match, we obtained a match to within the 2 σ errors of the observations for a shell model with $T_{\mathrm{eff}} =$ 50,000 K and $N = 3$ cm^{-3}. This model indicated a -3.5% correction to He/H—that is, the He^+ region was larger than the H^+ region, as is common for H II region models with hot ionizing stars. All of the model nebulae with $N = 10$ cm^{-3} had [O III] and [Ne III] line strengths far too low to match the observations. The results from the various models are illustrated in Figure 2.

How does the change in geometry affect the ionization correction factor (ICF) for helium? Despite the much lower ionization of the heavy elements in the shell models, the helium ionization changes very little at fixed T_{eff}. For the different models with $T_{\mathrm{eff}} \geq 37{,}500$ K, the helium ICF remained within $\pm 3\%$ of unity. Only for T_{eff} smaller than 37,500 K did the He ICF become larger than 1.1, as illustrated in Figure 3. Note the rapid increase in the ionization of helium for $T_{\mathrm{eff}} > 35{,}000$ K in Figure 3. The maximum ICF for helium obtained from the models was about 1.2, for $T_{\mathrm{eff}} = 35{,}000$ K; however, all of the 35,000 K models produced too little [O III] and [Ne III] to be acceptable. We note that spherical models with a small filling factor give similar results to the shell models.

We also note that several other factors affect the ICF for helium. One is the composition of the stellar atmosphere. The Mihalas (1972) stellar fluxes are supposed to be appropriate for a metal-rich case. However, the pure H-He stellar atmosphere models of Auer & Mihalas (1972) produce more He-ionizing photons and thus result in a smaller ICF for helium: for $T_{\mathrm{eff}} =$ 35,000 K, the model with the Auer & Mihalas stellar fluxes gave a neutral He fraction of only 10%, compared to 15% obtained with the Mihalas (1972) fluxes. Another factor is the treatment of the atmosphere models; the more realistic extended spherical non-LTE atmosphere models (e.g., Gabler et al. 1992) produce more hard ionizing photons than the older plane-parallel models, which would also increase the ionization of He.

Another method, suggested by Ali et al. (1991), uses the [Ne III]/[O II] ratio to measure the hardness of the radiation field. Although this method is somewhat sensitive to the assumption that Ne/O does not vary greatly from the solar neighborhood value and on the stellar atmosphere model fluxes used to compute photoionization models, our value of [Ne III]/[O II] $= 0.11 \pm 0.03$ and our photoionization models indicate a neutral He fraction of less than 15% with LTE stellar fluxes for effective temperatures greater than 35,000 K. This is illustrated in Figure 4. (The Ne^{++}/O^{++} ratio we derive yields a Ne/O abundance ratio which is consistent with the solar system ratio.) This is consistent with our other estimates of the neutral helium components.

To summarize, the various observational properties of H681 combined with the ionization model results lead us to conclude

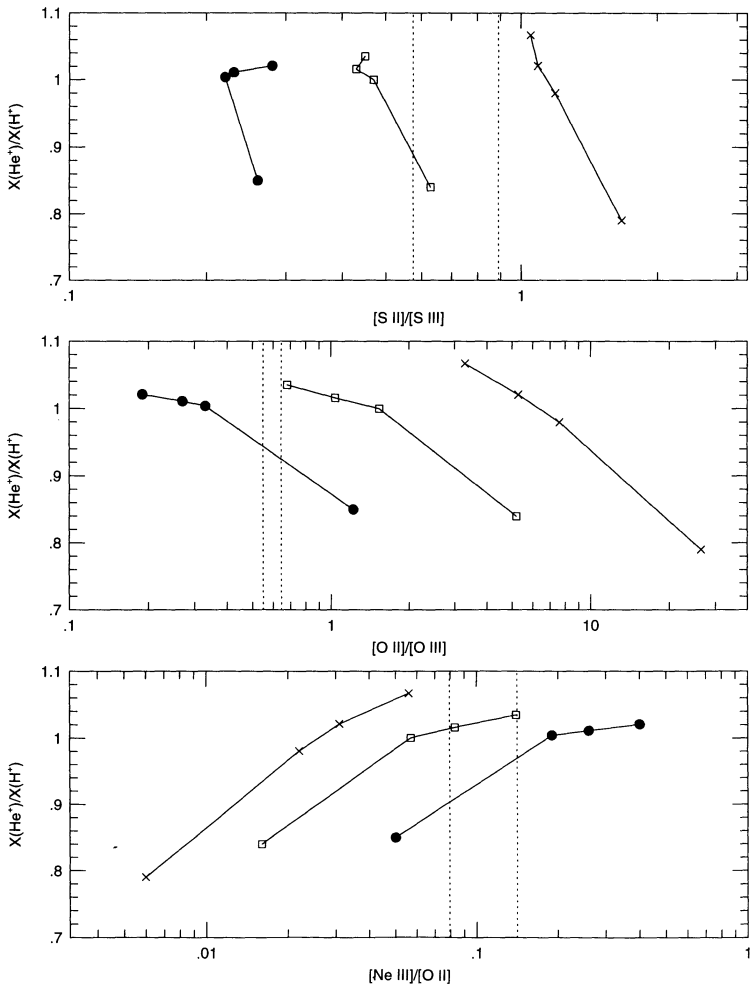

FIG. 2.—The ratio of the He^+ and H^+ volumes from photoionization models, as described in the text, vs. [S II]/[S III] (*top*), [O II]/[O III] (*middle*), and [Ne III]/[O II] (*bottom*). The filled circles represent uniform spherical models, open squares represent thin-shell models with $N = 3$ cm^{-3}, and crosses thin-shell models with $N = 10$ cm^{-3}. The lowest points along the sequences in each panel are models with 35,000 K ionizing stars; $T_{\rm eff}$ increases upward along each curve through 37,500 K, 40,000 K, and 50,000 K. The 1 σ observed range for each line ratio in H681 lies between the vertical dotted lines in each panel.

that the ionization correction for helium is not larger than 15%. Our measured value for the η parameter suggests hot ionizing stars. The strength of the [Ne III] emission leads us to a stellar effective temperature that is certainly greater than 35,000 K. Then, the diffuse structure and relatively large [O II]/[O III] and [S II]/[S III] ratios of the nebula lead to models with shell structures or a small filling factor; these models then require hotter stars which lead to small ionization corrections for helium. Given the uncertainties, we adopt a helium ICF = 1.05 ± 0.10. When we do this, we get He/H = 0.074 ± 0.010, or $Y = 0.228 \pm 0.031$.

3. DISCUSSION

Our basic result for H681 is that O/H = 8.4×10^{-5}, one-tenth the solar system oxygen abundance (Anders & Grevesse 1989), and 25% lower than the oxygen abundance in NGC 5471. This is not a remarkably low value in itself; many H II regions having much lower abundances have been found in dwarf emission-line galaxies. However, such low abundances have rarely been found in spiral disk H II regions. Typically, the lowest oxygen abundances found in spirals have been of order O/H = $1.2–1.5 \times 10^{-4}$ (references can be found in Garnett & Shields 1987), and none have been lower than that observed in NGC 5471 (Torres-Peimbert, Peimbert, & Fierro 1989, hereafter TPPF). Garnett et al. (1992) found O/H $\approx 8 \times 10^{-5}$ in the H II region MA 1 in M33, but that result has a much higher uncertainty than our value for H681. Our result suggests that a directed search could find other H II regions in spirals with comparable or even smaller abundances.

In Figure 5 we plot the composition gradient in M101, including our result for H681; we use the abundances for the inner H II regions derived by Evans (1986) and TPPF for our comparison, It is clear from the figure that H681 continues the smooth progression of decreasing O/H with increasing radial distance in M101; in fact, H681 falls almost perfectly on the log-linear relation defined by the inner H II regions (Evans 1986).

H681 was also observed as part of the H II region survey of Scowen, Dufour, & Hester (1992); H681 is clearly visible as the object at $R = 32.6$ kpc, 12 + log O/H = 8.2 in their Figure 5*a* (P. A. Scowen, private communication). The 0.3 dex discrepancy between their oxygen abundance and ours can be attributed to their use of [O III]/Hβ alone as an abundance

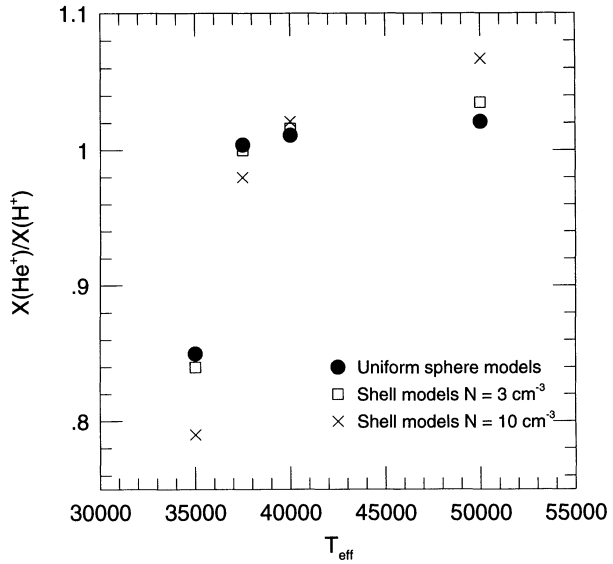

FIG. 3.—The ratio of the He^+ and H^+ volumes from photoionization models vs. stellar effective temperature. Symbols are as in Fig. 2. Note the rapid increase in the He ionization between $T = 35{,}000$ K and $T = 37{,}500$ K.

indicator. H681 occupies the regime where [O III]/Hβ yields two values for the oxygen abundance from the calibration diagrams of Edmunds & Pagel (1984); without another diagnostic to discriminate between the two values (such as electron temperature, or the strength of the [N II] lines), it is not possible to use [O III]/Hβ to uniquely determine O/H. From our results for H681, we suspect that the rise in O/H at $R > 25$ kpc seen in Figure 5 of Scowen et al. (1992) is an artifact of their choice of abundance indicator.

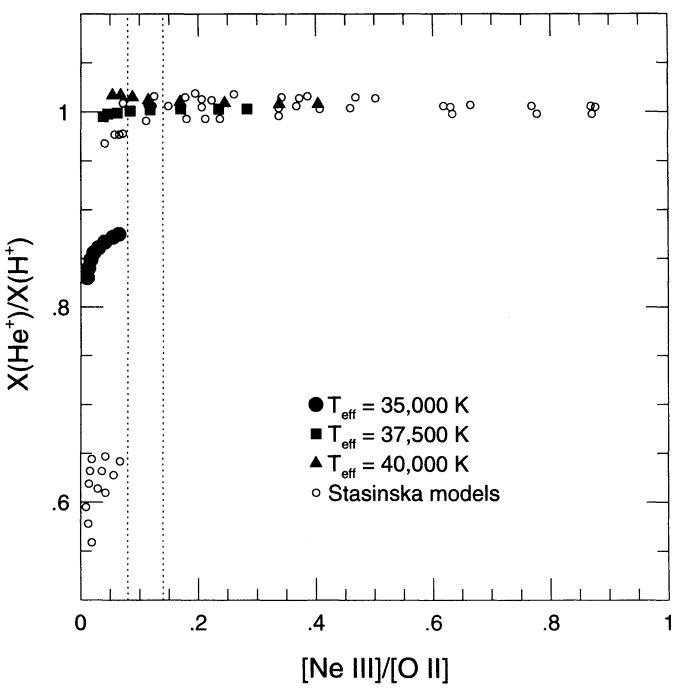

FIG. 4.—$X(He^+)/X(H^+)$ vs. [Ne III] λ3869/[O II] λ3727 from photoionization models as described in the text. The observed [Ne III]/[O II] ratio and its uncertainty is denoted by the region between the vertical dotted lines.

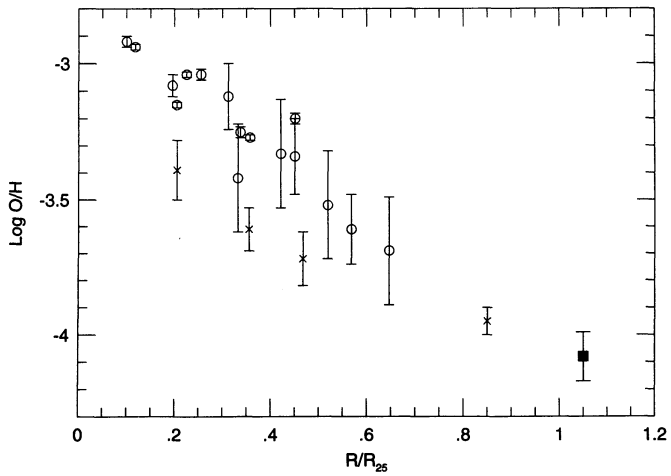

FIG. 5.—Log oxygen abundance for H II regions in M101 vs. galactocentric radius in units of the photometric radius. The filled square represents H681. *Open circles:* Evans (1986); *crosses:* TPPF.

The S/O ratio for H681 is plotted in Figure 6, along with other measurements of S/O in M101 from TPPF, Garnett (1989), Díaz et al. (1993), and Shields & Searle (1978, as reanalyzed by Garnett 1989). Given the relatively large uncertainty in the sulfur abundance, we conclude that S/O in H681 is essentially identical to the solar system ratio (Anders & Grevesse 1989). Although the data appear to show a slight trend of increasing S/O with increasing O/H, the uncertainty in the abundances and the heterogeneous nature of this data set force us to conclude at present that there is no evidence for any correlation. We have data for a much larger sample of H II regions in M101 which we will use to look at this question in greater detail.

We display the data for N/O and the He mass fraction Y in Figures 7 and 8, along with measurements for other M101 H II regions from TPPF. Again, our data for H681 continue the smooth trends in N/O and Y observed in the inner disk of M101. Notably, the value of N/O in H681 lies squarely in the

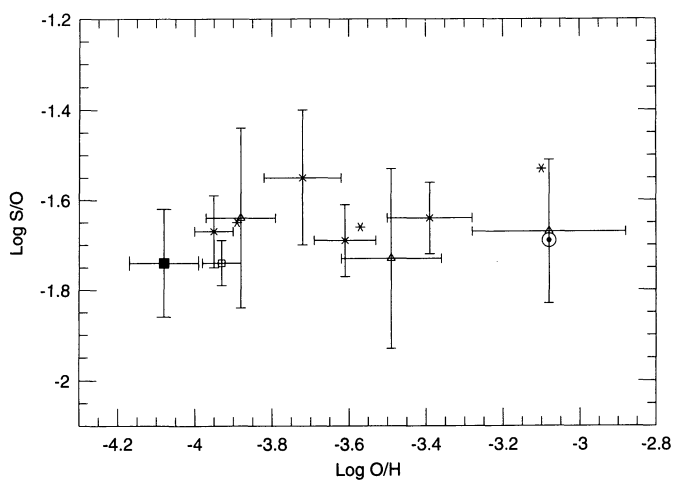

FIG. 6.—The ratio of the sulfur abundance to the oxygen abundance for M101 H II regions, plotted against O/H. The solar value is represented by the Sun symbol. The filled square represents H681. *Crosses:* TPPF; *open triangles:* Shields & Searle (1978), as reanalyzed by Garnett (1989); *asterisks:* Díaz et al. (1993).

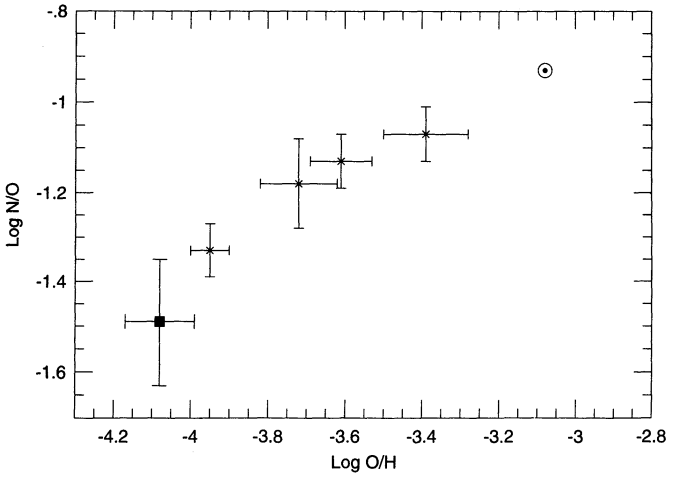

FIG. 7.—The ratio of the nitrogen abundance to oxygen abundance for M101 H II regions vs. O/H. Symbols are as in Figs. 5 and 6.

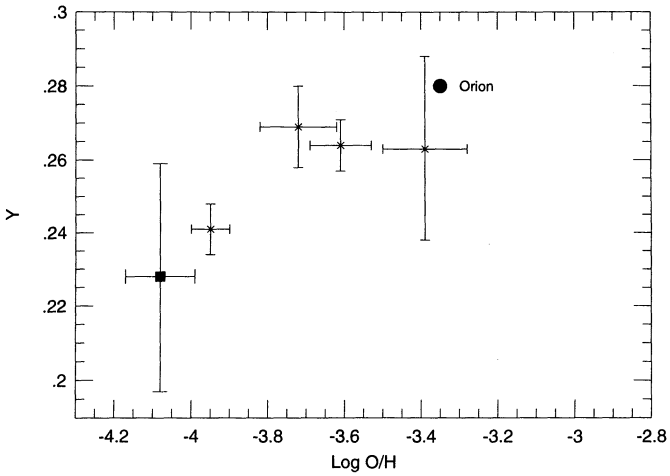

FIG. 8.—The helium mass fraction in M101 H II regions as a function of O/H. Symbols are as in Figs. 5 and 6. The filled circle represents the Orion Nebula.

range of values observed in dwarf emission-line galaxies. Our value of log N/O = −1.49 is very close to the mean value of −1.46 in dwarf galaxies (Garnett 1990). Unfortunately, the uncertainty in our He abundance does not constrain the abundance very well, but our derived value for Y in H681 is similar to that observed in dwarf galaxies having comparable O/H (Pagel et al. 1992). This suggests that the evolution of the outer parts of spiral disks and that of dwarf galaxies may bear some similarities. For instance, it has been suggested that gravitational potential may play a role in determining the chemical composition (Rubin, Ford, & Whitmore 1984). Regions of high gravitational potential may be better able to retain gas that has been energized by supernova events, and so can produce more generations of stars which enable helium and secondary nitrogen to increase with respect to oxygen. This process has been invoked to explain the properties of dwarf galaxies as well (e.g., Dekel & Silk 1986).

On the other hand, our observations do not appear to support the model of Charlton & Salpeter (1989; CS), in which metal-rich gas from a galactic fountain is redistributed across a disk galaxy. Their model predicts that some of the enriched fountain gas will travel out toward the edge of the disk, fall in and mix with only a small amount of pristine gas. This leads to an abrupt increase in the metallicity in the outer parts of the disk, depending on the amount of disk material that has been processed through the fountain. The illustrative model in Figure 4 of CS shows the increase in metallicity occurring between 1.5 and 2 times the half-mass radius of the disk. If we assume that the light traces the disk mass in M101 (ignoring the effects of the small bulge), then the effective radius R_e should approximate the half-mass radius. From the RC3, $R_e = 0.5A_e = 5'.7$ for M101, corresponding to 12.4 kpc at the assumed distance of 7.4 Mpc. Thus, H681 is located at 2.6 R_e. We do not see the expected increase in abundance. The model could be reconciled with our observation if very large amounts of disk material have been processed through fountains, but this tends to give shallow abundance gradients in the CS picture. It may be also that we have seriously underestimated the half-mass radius of the disk for M101. A stronger test of the CS model would be to observe interstellar absorption lines in the spectra of QSOs at more extreme radial distances than we can reach with H II regions.

To summarize, we have found that abundances in the outer parts of spiral disks can reach values significantly lower than found previously, comparable to the abundances observed in low-luminosity dwarf galaxies. A more extensive comparison of outer spiral disks and low-luminosity irregulars could yield important clues regarding the evolution of these different systems.

We thank the MMT operators, Carol Heller, John McAfee, and Janet Robertson, for their assistance in obtaining these observations. Thanks go also to Rene Walterbos and Robert Braun for sharing the CCD observations of M101, and Claus Leitherer and Evan Skillman for supplying references on He I line strengths in stars. Support for D. R. G. is provided by NASA through grant HF-1030.01-92A awarded by Space Telescope Science Institute, which is operated by the Association of Universities for Research in Astronomy, Inc., for NASA under NAS 5-26555. R. C. K. was supported by the National Science Foundation through grant AST 90-19150.

REFERENCES

Ali, B., Blum, R. D., Bumgardner, T. E., Cranmer, S. R., Ferland, G. J., Haefner, R. I., & Tiede, G. P. 1991, PASP, 103, 1182
Anders, E., & Grevesse, N. 1989, Geochim. Cosmochim. Acta, 53, 197
Auer, L. H., & Mihalas, D. 1972, ApJS, 24, 193
Blair, W. P., Kirshner, R. P., & Chevalier, R. A. 1982, ApJ, 254, 50
Charlton, J. C., & Salpeter, E. E. 1989, ApJ, 346, 101 (CS)
Clegg, R. E. S. 1987, MNRAS, 229, 31P
Conti, P. S. 1973, ApJ, 179, 161
———. 1974, ApJ, 187, 539
Conti, P. S., & Frost, S. A. 1977, ApJ, 212, 728
Dekel, A., & Silk, J. 1986, ApJ, 303, 39
de Vaucouleurs, G., de Vaucouleurs, A., Corwin, H. G., Jr., Buta, R. J., Paturel, G., & Fouqué, P. 1991, Third Reference Catalog of Bright Galaxies (New York: Springer-Verlag) (RC3)
Díaz, A. I., Terlevich, E., Pagel, B. E. J., Vílchez, J. M., & Edmunds, M. G. 1993, in Dynamical and Chemical Evolution of Galaxies, ed. J. J. Franco, F. Matteucci, & F. Ferrini, in press
Edmunds, M. G., & Pagel, B. E. J. 1984, MNRAS, 211, 507
Evans, I. N. 1986, ApJ, 309, 544
Gabler, R., Gabler, A., Kudritzki, R.-P., & Méndez, R. H. 1992, A&A, 265, 656
Garnett, D. R. 1989, ApJ, 345, 282
———. 1990, ApJ, 363, 142

Garnett, D. R. 1992, AJ, 103, 1330
Garnett, D. R., Odewahn, S. C., & Skillman, E. D. 1992, AJ, 104, 1714
Garnett, D. R., & Shields, G. A. 1987, ApJ, 317, 82
Hodge, P. W., Gurwell, M., Goldader J. D., & Kennicutt, R. C., Jr. 1990, ApJS, 73, 661
Hummer, D. G., & Storey, P. J. 1987, MNRAS, 224, 801
Kennicutt, R. C., Jr. 1978, Ph.D. thesis, Univ. Washington
———. 1984, ApJ, 287, 116
Mathis, J. S. 1982, ApJ, 261, 195
McCall, M. L., Rybski, P. M., & Shields, G. A. 1985, ApJS, 57, 1
Mihalas, D. 1972, Non-LTE Model Atmospheres for B and O Stars (NCAR TN/STR-76)
Olofsson, K. 1993, A&A, submitted
Osterbrock, D. E. 1989, Astrophysics of Gaseous Nebulae and Active Galactic Nuclei (Mill Valley: University Science Books)
Pagel, B. E. J., Simonsen, E. A., Terlevich, R. J., & Edmunds, M. G. 1992, MNRAS, 255, 325
Peimbert, M., & Costero, R. 1969, Bol. Obs. Tonantzintla y Tacubaya, 5, 3
Rubin, V. C., Ford, W. K., Jr., & Whitmore, B. C. 1984, ApJ, 281, L21
Sandage, A., & Tammann, G. A. 1976, ApJ, 210, 7
Scowen, P. A., Dufour, R. J., & Hester, J. J. 1992, AJ, 104, 92
Sedwick, K. E., & Aller, L. H. 1981, Proc. Natl. Acad. Sci., 78, 1994
Shields, G. A. 1987, in Proc. 13th Texas Symposium on Relativistic Astrophysics, ed. M. P. Ulmer (Singapore: World Scientific), 192
Shields, G. A., & Searle, L. 1978, ApJ, 222, 821
Skillman, E. D. 1985, ApJ, 290, 449
Stasińska, G. 1990, A&AS, 83, 501
Torres-Peimbert, S., Peimbert, M., & Fierro, J. 1989, ApJ, 345, 186 (TPPF)
Viallefond, F., Allen, R. J., & Goss, W. M. 1981, A&A, 104, 127
Vílchez, J. M., & Pagel, B. E. J. 1988, MNRAS, 231, 257